Journal of Materials Chemistry B

Accepted Manuscript

ROYAL SOCIETY OF CHEMISTRY

www.rsc.org/materialsB

Journal of Materials Chemistry B RSCPublishing

ARTICLE

Synthesis of radical mesoporous bioactive glass particles to deliver osteoactivin gene

Cite this: DOI: 10.1039/xoxxoooooox

Xian Li,[a,b,c] Xiaofeng Chen,*[a,b,c] Guohou Miao,[a,b,c] Hui Liu,[a,b,c] Cong Mao,[a,b,c] Guang Yuan,[a,b,c] Qiming Liang,[a,b,c] Xiongjun Shen,[a,b] Chengyun Ning[a,b] and Xiaoling Fu[a,b,c]

Received ,
Accepted

DOI: 10.1039/xoxxoooooox

www.rsc.org/

Mesoporous bioactive glasses (MBGs) can be used as carriers for biomolecule delivery with improved functions. Although there are a great number of studies on drug delivery by MBGs, till now, little work has been done to investigate the DNA gene transfection effect of MBGs. In this study, radial mesoporous bioactive glasses (rMBGs) were prepared by sol-gel process combining micro-emulsion method. The surface is further modified by amino groups in order to improve its affinity for DNA. Our study showed that rMBGs have good apatite-forming ability and cellular biocompatibility. Besides, rMBGs can enter cells in a time- and dose-dependent manner, and mainly localize in the cytoplasm. Agarose gel electrophoresis demonstrated pOA-EGFP (containing the osteoactivin and the green fluorescent protein fusion gene) can be completely absorbed and protected from DNase I degradation by the aminated rMBGs. Additionally, the plasmid can be successfully expressed in cells transfected by rMBGs.

1 Introduction

With the rapid development of bone tissue engineering in recent years, osteoinductive bone repair materials have been clinically used extensively.[1,2] Among those, bioceramics materials, such as hydroxyapatite (HA), calcium phosphates, bioactive glasses(BG), and related composite materials, are widely used for application in bone tissue engineering.[3,4] Bioactive glass, first developed by Hench and co-workers in 1969,[5] has higher rate of bone formation compared with other inorganic ceramics such as hydroxyapatite.[6,7] BG has become an important inorganic biomaterial for bone and dental restoration.[3,8] More and more attention has been paid on the study of BG.

BG has excellent biocompatibility and biological mineralization, due to the chemical reactions on the material surface.[7,9-11] Ion dissolution products released from BG can result in active apatite surface layer,[12-14] up-regulation of osteogenic gene expression,[15-17] stimulation of osteoblast proliferation and differentiation,[15,16] increasing secretion of vascular endothelial growth factor (VEGF).[18-20] These typical characteristic and favorable responses of BG contribute to its bioactivity and promote rapid bone formation. Nowadays, BG is widely used in orthopedics and stomatology,[7,21] because of its high apatite-forming bioactivity, biodegradation, angiogenic properties and good abilities.

The 45S5 bioglass, considered as the gold standard of BG, is a dense massive material with a low specific surface area, which is fabricated by the traditional melt-derived approach.[4,8] However, melting process has a number of limitations, for example, the high processing costs, lack of microporous structure inside the materials, low specific surface area.[4,7] Sol–gel process firstly reported in the early 1990s offers an alternative method to prepare BG.[22] With relatively low temperatures, Sol-gel process offers many potential advantages compared with melt approach, including easier to achieve powders with specific size ranges, better to control the purity and bioactivity, and a relative higher specific surface area.[4,21]

About a decade ago, a new type of BG, called mesoporous bioactive glasses (MBGs), was developed by Yan and co-workers,[23] through combination of the sol–gel method and the supramolecular chemistry of surfactants. MBGs possess uniform and adequate mesoporous, controllable nanopore size and pore volume, excellent cytocompatibility and apatite mineralization.[24-26] Because of the super characters, the study of MBGs for biomolecular delivery and bone tissue engineering has been attracted more and more attention.[27,28] MBGs have been prepared as particles, spheres, or other structures by combinations of structure-directing agents and special techniques.[23,27,29-31] Cetyltrimethyl ammonium bromide (CTAB), F127 (EO106-PO70-EO106) and P123 (EO20-PO70-EO20) are three important kinds of structure-directing agents. It was found that CTAB-induced MBGs has higher loading efficiency than F127 or P123 induced MBGs, for a smaller mesopore size of CTAB-induced MBGs.[27] So the mesoporous structures, preparation methods, and even the dissolution of MBGs are extremely important to influence the biomolecule delivery.

Based on the attractive properties, MBGs have attracted increasing attention and received much interest.[27,32] The important potential application of MBGs is that it can load and deliver biomolecules,[27,31] such as chemical drugs, siRNA, etc.[31,33] Nano bioactive glass loaded doxorubicin can effectively inhibit the proliferation of bone tumor cells.[34] Incorporation of yttrium in BGs leads to a new generation of radionuclide vectors for cancer therapy.[35] Functionalized MBGs with folic

acid (FA) were evaluated specifically for targeting cancer cells.[36] Wu et al.[27] reported a dexamethasone delivery system using well-ordered MBGs as carriers and revealed a significant enhance osteogenesis. Our previous report suggested that micro nano BGs promote osteoblast differentiation and new bone formation, and MBGs through controlled release of alendronate sodium.[28,31,32] MBGs is also an excellent carrier of ampicillin for anti-bacteria application.[33,37] VEGF released MBG scaffolds improved the viability of endothelial cells.[38,39] Delivery of rhBMP-2 by MBGs significantly promoted the osteogenic differentiation of MSCs.[40-42] Mesoporous bioactive glass nanoparticles have been reported as siRNA carriers.[33] The siRNA–BG nanoparticles were easily taken up by the cells, with a transfection efficiency as high as 80%. These studies suggest that MBGs holds great promise for biomolecule delivery with improved functions. Although there are studies for the delivery of biomolecules by MBGs, till now, little work has been done to investigate the DNA gene transfection function of MBGs, which may be very important for developing new type of bone restoration materials with gene mediation function for bone regeneration application.

Generally, gene delivery vectors can be divided into viral and non-viral ones. Viral vectors are efficient, but they are potentially dangerous because of their severe immune/inflammatory reactions in patients. Non-viral vectors, such as lipids, polymers, calcium phosphate nanoparticles, modified mesoporous silica nanoparticles, offer several advantages including low immune toxicity, construction flexibility and facile fabrication, and have attracted much interest.[43-48] However, the use of MBGs for DNA gene delivery has not been reported. In this study, rMBG particles, with unique radial and fibrous structure, controllable pore architecture, good dispersion and excellent mineralization ability, were developed as gene vectors. Physicochemical properties, apatite-forming ability and cellular biocompatibility, as well as the gene-delivering ability were investigated. Osteoactivin (OA) was chosen as a model gene, which can induce the differentiation of osteoblasts.[49] The gene loading capacity and transfection efficiency of rMBGs were discussed.

2 Materials and methods

2.1 Reagents and instruments

Human 293T and Hela cell lines were preserved by our lab. Dulbecco's modified Eagle medium (DMEM), trypsin and fetal bovine serum were obtained from Gibco Co. (USA). Fluorescein isothiocyanate (FITC), Rhodamine and Deoxyribonuclease I were obtained from Sigma Co. (USA). Tetraethyl orthosilicate (TEOS), triethyl phosphate (TEP), $Ca(NO_3)_2$ $4H_2O$, cetyl pyridine bromide(CPB) and urea were purchased from Guangzhou Chemical Reagent Factory Co. Ltd (China). Mammalian cell expression vector pAc-EGFP-N1 was provided by Clonetech Co. (USA). pCMV-Sport6-OA was purchased from Thermo company (USA). All primers were made by Sangon Biotech (Shanghai) Co., Ltd. (China). Lipofectamine ™ 2000 was purchased from Invitrogen (Carlsbad, CA, USA). The microscope was from Zeiss Co. (Germany). Flow cytometry (BD FACSAriaTM) analyzer was from BD Co. (USA). 2-(4-Amidinophenyl)-6-indolecarbamidine dihydrochloride (DAPI) Staining Solution was purchased from Beyotime Institute of Biotechnology (China).

2.2. Preparation of radical mesoporous BG nanoparticles

Radical mesoporous bioactive glass (rMBG) nanoparticles(80mol%SiO_2, 20mol%CaO,80S20C) were prepared by sol-gel process combining micro-emulsion method and gelation-induced phase separation technology according to a modified method[50]. The process of peparing rMBG particles is as follows: 0.6 g of urea and 1 g of CPB were dissolved in 30 ml of deionized water under vigorous stirring. After that, 30 ml of cyclohexane and 0.92g of iso-propanol were added, after stirring for 2 h, a homogenous milky solution was obtained, and then 2.7 ml of TEOS was added dropwise to the solution and hydrolyzed for 30 min at room temperature. Afterwards, the reaction temperature was set at 70℃. 0.71g of calcium nitrate as calcium precursor was added after 8 h of reaction, and the reaction was continued to 16 h. After the temperature cooled down, the resulted precipitates was collected by centrifugation at 10000rmp for 15 min, and washed three times with acetone and absolute ethanol, and twice with deionized water. The collected precipitates was freeze-dried for 48 h at -40℃ and calcined at 600 ℃ for 5 h to remove the residual organics with a heating rate of 1 ℃/min (Fig.1).

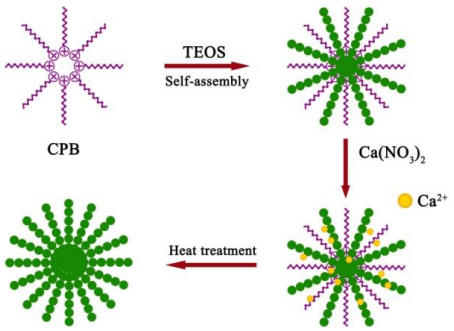

Fig.1. Schematic illustration of the synthesis of rMBGs

2.3. Preparation of amino modified rMBG (rMBG-NH_2) and FITC loaded rMBG (rMBG-FITC) nanoparticles

150mg rMBG was dissolved in 100 mL of toluene, and then stirred at 80℃. Next, 1.5 mL aminopropyltriethoxysilane (APTES) was added and the reaction was continued for 16 h. The particles were washed by ethanol for more than five times , and dried at 60℃ for 48 h. rMBG-FITC was synthesized by dissolving 2 mg of fluorescein isothiocyanate (FITC) in 10 mL of distilled H_2O, and then 50mg rMBG-NH_2 was added. The mixture was stirred at room temperature in darkness for 2 h. Precipitate was collected by centrifugation at 10000rmp for 15 min, and washed several times with deionizer water until the fluoresces couldn't be detected in the supernatant.

2.4 Characterizations of rMBG nanoparticles

The morphology of the mesoporous BG nanoparticles was observed by a scanning electron microscopy（Zeiss Ultra 55，Germany）. The particle size and mesoporous structure of the nanoparticles were also observed by a high-resolution transmission electron microscope using a JEM- 2100HR apparatus (JEOL, Japan). The specific surface area, pore volume, and pore size distribution were determined based on N_2 adsorption–desorption measurements. N2 adsorption/desorption isotherm was recorded at 77 KThe N_2

adsorption–desorption isotherms were obtained at 77 K using a pore size and surface area analyzer (NOVA 4200e, Quantachrome). Samples were degassed under vacuum at 250℃ for 4 h prior to analysis. The surface area was calculated by the Barrett–Emmett–Teller (BET) method and the pore size distribution was determined from the desorption branch of the isotherms by Barrett–Joyner–Halenda (BJH) method. Powder Fourier transform infrared spectroscopy (FTIR) analyses were performed on a Fourier transform infrared spectrometer (Nicolet Nexus, USA) using KBr pellet method in the scanning range of 4,000–400 cm^{-1}.

2.5 Apatite-mineralization of the rMBGs

rMBG particles were soaked in simulated body fluid (SBF) medium and were placed in a shaking incubator with a constant shaking speed of 120 rpm at 37 ℃. The ratio of rMBG weight to solution volume of SBF was 1.0 mg/mL. After soaking for 7 days, the samples were collected by filtration, rinsed by acetone and deionized water three times, respectively, and then dried at 60℃C for 1 day. The apatite formed on the surface was characterized using SEM and FTIR.

2.6 Construction of pOA-EGFP

A full-length OA sequence was found in the universal GenBank database (AF184983) and was purchased from Thermo company (vector: pCMV-Sport 6-OA). Oligonucleotide couples used for PCR were FW: 5'--- ccg ctcgag atg gaa agt ctc tgc ggg g---3' and RV: 5 ---- ccc aagctt gag cat cca tgg ctt gtc ctg---3', in order to amplify fragments OA. The resulting products were digested with XhoI /HindIII, and then cloned into the mammalian cell expression vector pAc-EGFP-N1. Plasmids were verified by PCR, enzyme digestion and sequence analysis until the results showed that the gene sequence was correct.

2.7 Zata potential measurement

100μg of rMBG-NH_2 was soaked in 1 mL deionizer water, and then different amount of pOA-GFP(1, 2, 3, 4, 5, 6μg) were added separately. The mixture was incubated for 30 minutes and collected by centrifugation, and then zata potential was measured (Zetasirer nano ZS).

2.8 Gene loading efficiency and gene protection of rMBG

pOA-GFP was added in different amount of rMBG-NH_2 (rMBG-NH_2/ pOA-GFP mass ratio= 0, 10, 30, 50, 70, 100) separately. The total volume of the reaction system was 300 μL, and the initial concentration of pOA-GFP was 3.3μg/μL. The mixture was incubated for 30 minutes in a shaker at room temperature, and then 20 μL was taken out to detect by gel electrophoresis. Other mixture was centrifugated at 10000rmp for 5 min, plasmid concentration in supernatant was detected by Nanodrop 3300. The absorption efficiency was calculated as: absorption efficiency (%)=[(initial plasmid concentration - supernatant plasmid concentration)/ initial plasmid concentration]×100%.

After incubated for 30 minutes in a shaker, the rMBG-NH_2 and pOA-GFP mixture was centrifugated, and the supernatant was discarded. The pOA-GFP loading rMBG-NH_2 complex (rMBG-NH_2/pOA-GFP) was resuspended in 10 μL deionized water. 5 μL deoxyribonuclease I (DNase I, 50U/μL) and 5 μL reaction buffer were added. rMBG-NH_2/pOA-GFP was incubated in a thermostat-controlled waterbath for 30 min and the digestion was blocked by 5μL EDTA. Gene protection of rMBG was studied by gel electrophoresis. pOA-GFP incubated with or without DNase I was taken as the positive or negative control.

2.9 Cell culture and proliferation assay.

Cells were cultured in DMEM medium (Gibco, USA) supplemented with 10% fetal bovine serum, at 37℃ in a 5% CO_2 incubator. The effect of the rMBG particles on proliferation of cells was determined by the CCK8 assay. Cells cultured in 96-well plates were treated with different rMBG particles for 48 h at 37℃. A 10 μL volume of CCK8 was added to each well and cells were incubated for another 4 h. The absorbance was measured at 450 nm using amicroplate reader (Thermo 3001, Thermo Co., USA). Three specimens for each culture time point were tested and each test was performed in triplicate. The proliferation of the cells was expressed as: relative cell proliferation rate = (experimental group absorbance - background absorbance) / (control absorbance - background absorbance) × 100%.

2.10 rMBG particles entering cells

2.10.1 Flow cytometry detection

Hela cells were cultured for 24 h in 6-well plates at an initial density of 1×10^5 cells per well. To analysis the process of rMBG entering cells, a time course study was performed by stimulating cells with different concentrations of rMBG-FITC (0, 10, 20μg/mL) and harvesting them at 3 h and 24 h. Cells were washed twice with phosphate buffer solution (PBS), the cell concentration was adjusted to 1×10^6 /mL and fluorescence was measured by flow cytometry (BD FACSAriaTM). The experiments were done in triplicates for each group and the mean value of FITC-COS fluorescence of each group was calculated.

2.10.2 TEM detection

Hela cells were cultured in 10 cm dishes, incubated with 10μg/mL rMBGs for 24 h, and then harvested. Cells were washed with PBS at room temperature for twice, centrifuged for 5 min at 1,000g at room temperature to form a pellet at the bottom of the capsule, and fixed by 1 mL 4%（w/v）glutaraldehyde. osmium tetroxide. 1 mL 1% osmium tetroxide was added to the cell pellet. Remove ddH_2O by dehydration through a graded series of ethanol concentrations (50, 70, 90 and 100%) for 5–15 min each. Cell pellet was resin embedded, sectioned, and stained with 1% uranyl acetate and lead citrate. Finally images were collected with a TEM(Tecnai G^2 Spirit Twin, USA).

2.10.3 Fluorescence microscopy detection

Hela cells were cultured in 24-well plates for 24 h. 20μg/mL rMBG-FITC were added and cultured for another 24 h. Cells were incubated with 300 μL DAPI nuclear staining for 5 min, washed by PBS, and then observed by fluorescence microscopy.

2.11Cell transfection

293T cells that were 40% confluent were incubated with Lipofectamine ™ 2000 and the pOA-GFP or pAc-GFP-N1 plasmid for 5 h, and then the medium was replaced with fresh culture medium. Different amount of pOA-GFP was added to the medium with different amount of rMBG-NH_2 particles (pOA-GFP was 5μg/mL, and the rMBG-NH_2/pOA-GFP ratio was controlled at 10, 20, 50 and 100 respectively by regulating the initial amount of rMBG-NH_2 concentration. rMBG-NH_2/pOA-GFP ratio was

controlled at 50, and the amount of pOA-GFP was 1, 3, 5, and 7μg/mL respectively.). The mixture was incubated for 30 minutes, and then was added to the culture medium for 5 h. After transfection for 48 hours, cells were then studied under a fluorescence microscope or a flow cytometry.

3 Results

3.1 Properties of rMBG particles

rMBG particles were successfully prepared by sol-gel process combining gelation-induced phase separation technology using CPB as a template. SEM and TEM analysis (Fig. 2a-c) showed that particles were spherical with an average size of 180 ±17 nm (Fig. 2d). Large agglomerates hadn't been observed, indicating rMBG particles had good dispersion. Revealed by TEM (Fig. 2c), the particles had a sea hedgehog-like morphology, with a dense core and loose radiating fibers around. Apparently, this special morphology ensured the particles plenty of internal nano-porous structures.

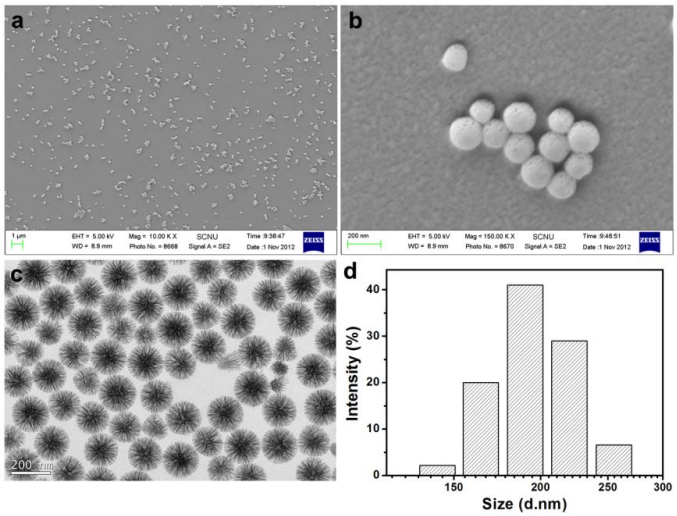

Fig.2. Characterization of rMBGs. (a) and (b)SEM images of rMBGs. (c) TEM morphologies and (d) particle size distribution of rMBGs.

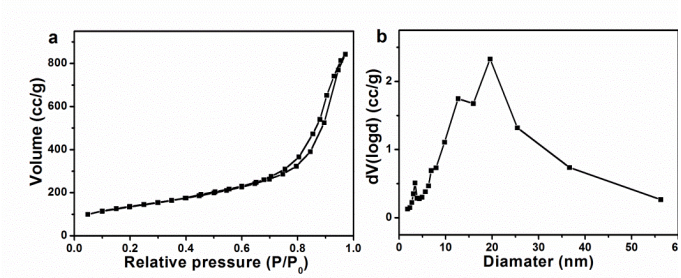

Fig.3. The pore structure and size of rMBGs. (a) N_2 isotherms. (b) Pore size distribution.

Table 1 Surface area, pore volume and pore size of rMBG particles

Sample(surfactants)	S_{BET} (m^2/g)	D_p (nm)	V_P(cm^3/g)
80S20C	483.98	10.77	1.30

The properties of mesoporous were also studied(Fig.3 and Table 1). The results of N_2 adsorption– desorption analyses of the particles showed that all materials had a type IV isotherm with H_3-type hysteresis loop (Fig. 3a), a typical characteristic of a mesoporous structure, indicating the materials possess a slit pore structure. The mesopore size of rMBG particles ranged from 10 to 30 nm (Fig. 3b). As shown in Table 1, the specific surface area, average pore size and total pore volume of all rMBG spheres were 483.98 m^2/g, 10.77nm and 1.3 cm^3/g respectively.

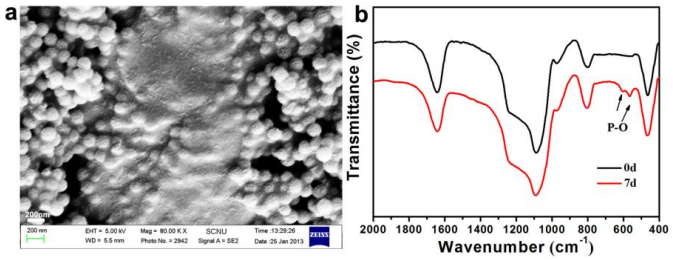

Fig. 4. Mineralization ability of rMBGs. (a)SEM (b)FTIR

3.2 Mineralization of rMBG particles

After immersed in SBF at 37°C for 7 days, a mineralized layer was formed on the surface of the rMBG particles (Fig.4a). FTIR analysis showed that compared with control, the weak double peaks, P–O bending vibrations of phosphate in crystalline phases, at 603 and 564 cm^{-1} appeared at 7 days, which indicated that the mineralized layer was composed of HA with a low crystallinity. These results suggested that rMBG particles possessed excellent apatite-mineralization formation properties.

3.3 Efficiency of rMNG particles entering cells

The surface of the rMBG particles and the plasmids had a negative charge. In order to increase the loading ability, rMBG particles were modified by amino groups (rMBG-NH_2) with silane coupling agents to obtain a positively charged surface. To study the labeling efficiency of rMBGs, rMBG-NH_2 particles were connected with FITC fluorescent marker (rMBG-FITC). rMBG-NH_2 and rMBG-FITC particles were put into PBS(20μg/mL), and then the fluorescence of the particles was tested by flow cytometry. Fig. 5 showed that the fluorescence of rMBG-FITC was higher than that of rMBG-NH_2. Scatter diagram moved to the right and FITC labeling efficiency of rMBG-NH_2 can reach more than 90%, which indicated that rMBG-NH_2 could interact with other biomolecules in a high efficiency.

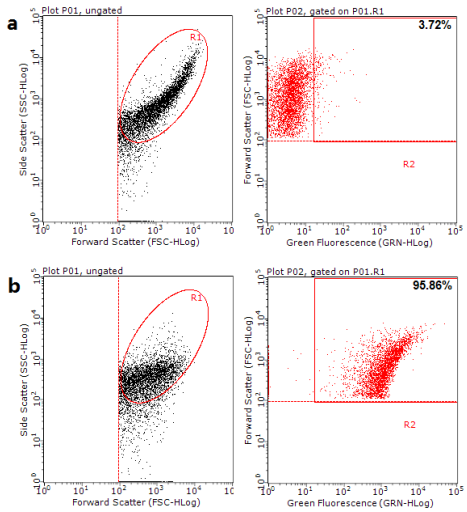

Fig.5. Labeling efficiency of rMBG-NH_2 particles studied by flow cytometry. (a) rMBG-NH_2 (b)rMBG-FITC

In order to determine whether the rMBG particles can enter into the cells, Hela cells were incubated with rMBG-FITC particles at different concentration for different time course. Fluorescence intensity was determined by flow cytometry after cells were co-cultured with 0, 10, 20, 50 μg/mL rMBG-FITC and harvested at different time points (3, 24 h,). According to our results, rMBG-FITC entered cells in a dose- and time-dependent manner. After incubated for 3 hours, many cells expressed FITC, and the 50ug/ml experimental group have higher positive expression amount than the 10 and 20 ug/ml groups. After 24 hours, more than 95% of the cells can be detected with FITC fluorescence (Fig.6), while little fluorescence was detected in rMBG groups and the control group. Fluorescent microscopy showed there were a large number of swallow bodies in the cells and most of the rMBG-FITC particles were located in the cytoplasm (Fig.7). TEM results were constant with those of the flow cytometry and fluorescent microscopy analysis. Fig. 8 showed that rMBG can successfully enter into the cells. Most of the particles were localized in the cytoplasm, and no particles were observed in nucleus. These results indicated that rMBG particles can enter the cells through phagocytosis.

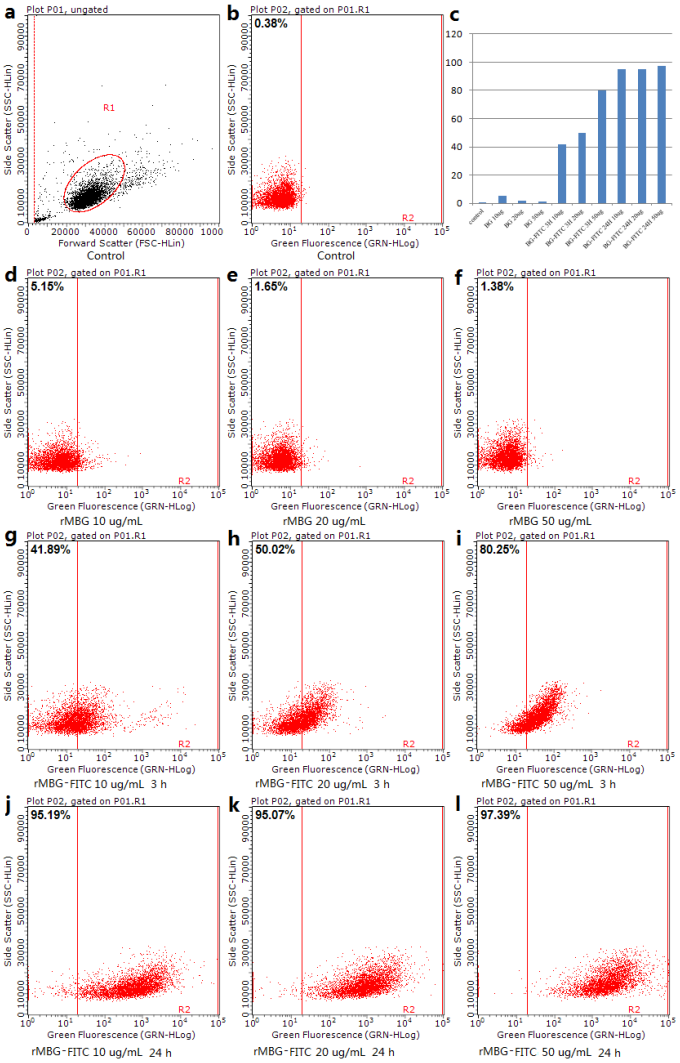

Fig. 6. Process of rMBG-FITC particles entering cells detected by flow cytometry.(a) and (b) Control.(c) Positive cells were quantitatively analyzed.(d) 10μg/mL,(e) 20μg/mL and (f)50μg/mL rMBG particles were incubated with cells for 24 h. (g) 10μg/mL,(h) 20μg/mL and (i)50μg/mL rMBG-FITC particles were incubated with cells for 3 h. (j) 10μg/mL,(k) 20μg/mL and (l)50μg/mL rMBG-FITC particles were incubated with cells for 24 h.

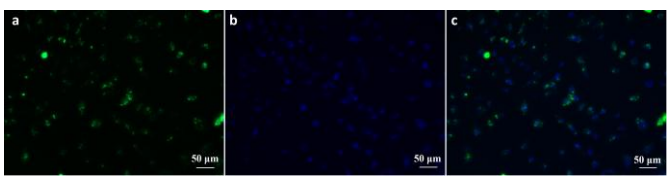

Fig.7. Fluorescent microscopy images of cells after incubated with rMBG-FITC. (a) rMBG-FITC; (b)DAPI; (c) Merge of (a) and (b).

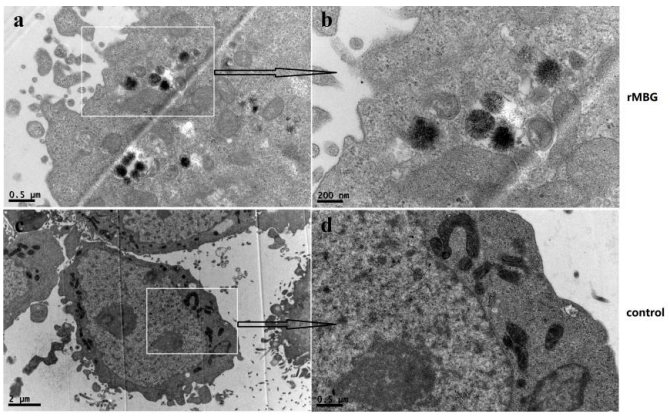

Fig.8. TEM ultrastructure of rMBG particles in Hela cells. (a) and (b) rMBG particles. (c) and (d)Control.

3.4 Gene loading

The unique radial pore structure and large surface area provided the rMBGs a promising potential application as carrier of molecules. Further, we carried out some preliminary experiments to investigate the possibility of rMBGs being used as gene transfection carriers. After amino modification, the zata potential of sample surface was about +23 mV (Fig.9). When the amount ratio of rMBG-NH_2 to pOA-GFP was turned from 100:1 to 50:1, the zata potential turned from a positive to a negative value. With the increasing amount of pOA-GFP, the surface potential materials/pOA-GFP composite decreased, which suggested that rMBG particles had a good loading ability of genes.

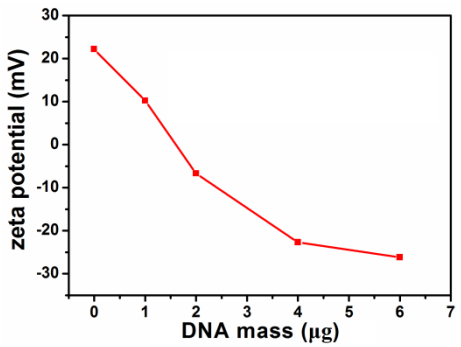

Fig.9. Zata potential of rMBG-NH_2/pOA-GFP. 100μg of rMBG-NH_2 particles were mixed with different amount of pOA-GFP (0, 1, 2, 4 or 6μg) in 1 mL denionized water respectively, and then the mixtures were incubated for 30 min before zata potential analysis.

Next, gene loading efficiency was detected by gel electrophoresis. pOA-GFP was added into different amount of rMBG-NH_2 (rMBG-NH_2/ pOA-GFP mass ratio= 0, 10, 30, 50, 70, 100) separately. The mixture was incubated for 30 minutes. From the gel electrophoresis principle, we learned that nude plasmid DNA could be seen in the gel. When some of the plasmid was adsorbed by the particles, DNA could be detected both in the gel and in the sample hole, because the glass particles could not move in the gel and the rMBG-NH_2/ pOA-GFP complex stayed in the sample hole. As the amount of the rMBG-NH_2/ pOA-GFP increases, the adsorption capacity of rMBG becomes stronger. pOA-GFP was fully adsorbed by rMBG-NH_2 when the rMBG-NH_2/ pOA-GFP mass ratio was up to 50:1(Fig.10), which explained that the plasmid was only detected in the sample hole. The loading efficiency was calculated through the plasmid concentration in the supernatant as described in chapter 2.8. As listed in table 2, pOA-GFP can be completely combined with rMBG-NH_2, when the mass ratio of rMBG-NH_2/ pOA-GFP was higher than 50:1, which was consistent with the result of zata potential.

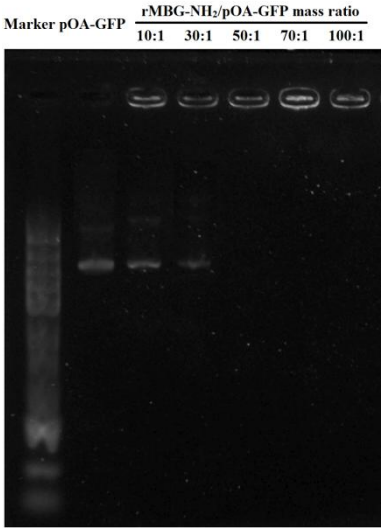

Fig.10. The pOA-GFP loading efficiency of rMBG-NH_2 particles

Table 2 The loading efficiency of pOA-GFP in rMBG particles

rMBG-NH_2/pOA-GFP (m/m)	Loading efficiency (%)
10	42.4±3.0
30	70.7±4.6
50	100
70	100
100	100

3.5 Gene protection of rMBGs

Cells contain many enzymes that can degrade DNA. The most common one is the nuclease. If the plasmid is degraded, it is incapable of replication and transcription, let alone translation into proteins. As a gene carrier, rMBGs were not only expected to have a high gene loading capacity, but also to maintain the stability of gene and keep it from degradation. In this study, gene protection of rMBGs was evaluated by using deoxyribonuclease I (DNase I), a nuclease that cleaves DNA preferentially at phosphodiester linkages adjacent to a pyrimidine nucleotide. Free plasmids were degraded after digestion for 30 min (Fig. 11 line 3), compare with the plamids without DNase I (Fig. 11 line 2). The rMBG-NH_2/pOA-GFP groups with or without DNase I were all stayed in the sample pore (Fig.11 line 4, 5, 6 and 7). pOA-GFP in the complexes was not degraded by DNase I (Fig.11 line 5 and 7), indicating that pOA-GFP was protected from enzymaitc digestion.

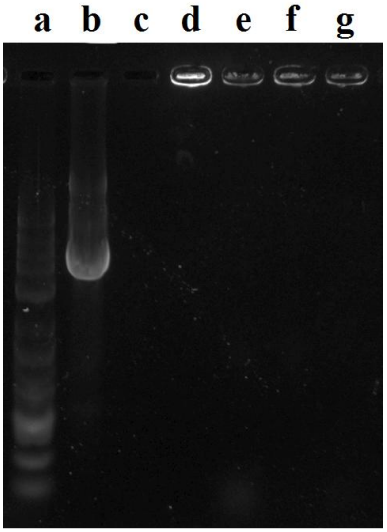

Fig. 11 rMBG-NH_2 particles protected pOA-GFP from enzymatic digestion.(a)Marker (b) pOA-GFP (c) pOA-GFP+DNase I (d) rMBG-NH_2/pOA-GFP (30:1) (e) rMBG-NH_2/pOA-GFP (30:1)+DNase I(f) rMBG-NH_2/pOA-GFP (50:1) (g) rMBG-NH_2/ pOA-GFP (50:1)+DNase I

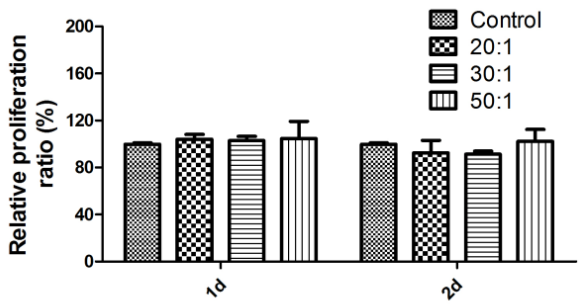

Fig.12. Effects of rMBG-NH_2/pOA-GFP mixtures (mass ratio=20, 30 or 50:1) on cell proliferation tested by CCK8.

3.6 Cell biocompatibility of rMBGs

We used the CCK8 assay to analyze the effects of rMBG-NH_2/pOA-GFP mixture on cell proliferation. Cells were incubated with different rMBG-NH_2/pOA-GFP (mass ratio= 20, 30 and 50) for 24 h and 48 h. We demonstrated (Fig. 12) that there was no significant change in the cells treated with rMBG-NH_2/pOA-GFP groups when compared with untreated control cells. rMBG-NH_2/pOA-GFP complexes exhibited a good cell biocompatibility at rMBG-NH_2/OA mass ratio of 20, 30 and 50.

3.7 Gene transfection of rMBGs

A microscope was used to determine the OA-GFP fluorescence intensity in 293T cells that were transfected with rMBG-NH_2/ pOA-GFP. Effects of the amount and the ratio of rMBG-NH_2/ pOA-GFP on transfection efficiency were discussed. The amount of pOA-GFP plasmid was at 5μg/mL, and rMBG-NH_2 was added to reach 10, 20, 50 and 100 mass ratio respectively. The positive control cells were transfected with pAc-GFP-N1 or pOA-GFP by lipofectamin ™ 2000 according to the manual. As shown in Fig.13, after transfected for 48 h, cells in pAc-GFP-N1 positive groups, exhibited a visible green fluorescence in the whole cells, while fluorescence was existed only in cytoplasm in pOA-GFP positive group (Fig.13a, b). In rMBG-NH_2/ pOA-GFP raio=10 group, these cells exhibited very weak intracellular fluorescence (Fig.13c). Cells treated with higher mass ratio of rMBG-NH_2/ pOA-GFP exhibited higher fluorescence intensity when compared with low mass ratio cells. The 50 ratio group achieved the best result. But when the mass ratio reached 100, fluorescence expression decreased(Fig.13). Next, rMBG-NH_2/pOA-GFP ratio was fixed at 50, and the amount of pOA-GFP plasmid and rMBG-NH_2 were adjusted. When the amount of pOA-GFP increased from 1 μg/mL to 7 μg/mL (rMBG-NH_2 amount increased from 50 μg/mL to 350 μg/mL accordingly), the fluorescence expression at first increased and then decreased, and pOA-GFP=5μg group had the best transfection effect (Fig.13). In conclusion, when the rMBG-NH_2/ pOA-GFP ratio=50 and the pOA-GFP=5 μg, the transfection efficiency of rMBGs was optimal.

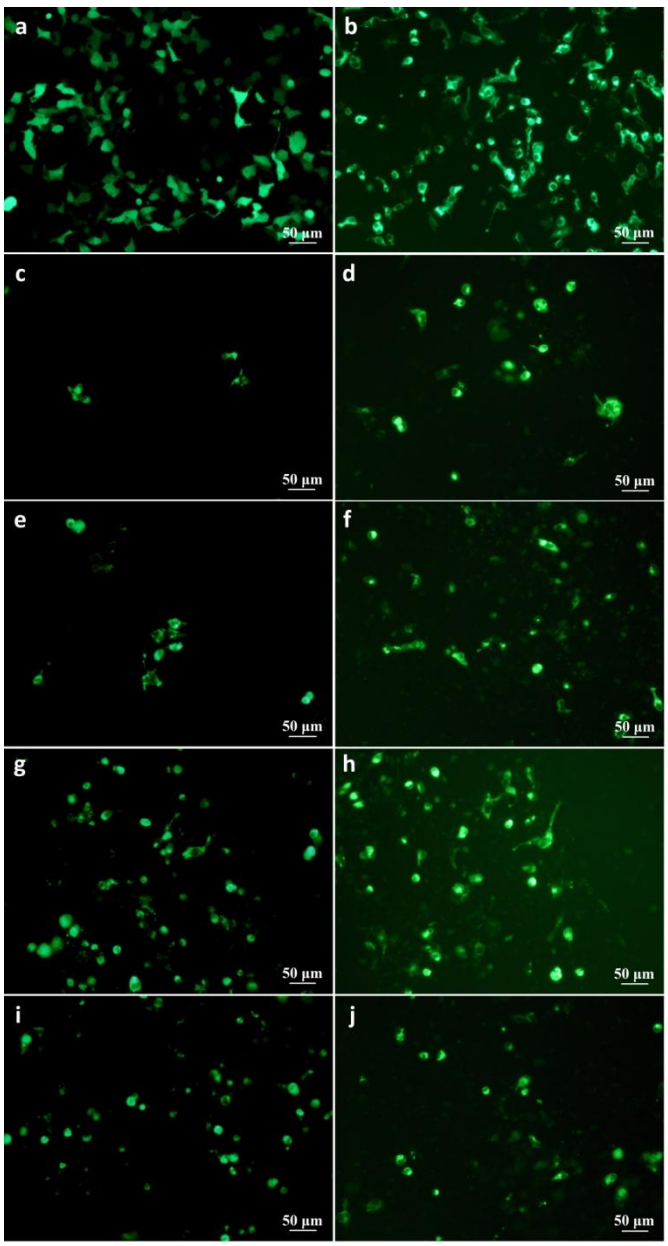

Fig.13. Expression of OA-GFP in 293T cells transfected by rMBG-NH_2. Fluorescent microscopy images of (a)GFP and (b) OA-GFP

transfected by lipofectamine ™ 2000. (c-j) Images of OA-GFP transfected by rMBG-NH_2. (c,e, g, i) pOA-GFP=5μg/mL, rMBG-NH_2/ pOA-GFP ratio=10, 20, 50 and 100 respectively. (d,f,h,j) rMBG-NH_2/ pOA-GFP ratio=50, pOA-GFP=1, 3, 5, and 7μg/mL respectively.

Flow cytometry was used to determine fluorescence intensity in 293T transfected cells (Fig.14). Control cells without treatment were used as a blank. Clearly, the graphs of positive pOA-GFP transfected group (transfection efficiency: 43.6±5.8%) and all the rMBG experimental transfected groupswere shifted to right. rMBG-NH_2/ pOA-GFP groups (transfection efficiency of rMBG-NH_2/ pOA-GFP ratio= 20, 50, 100 groups was 12.8±1.7%, 24.6±2.3% and 16.2±4.1% respectively) had higher fluorescence intensity than that in the control group (transfection efficiency: 3.5±0.8%), especially in the rMBG-NH_2/pOA-GFP ratio=50 experiment group, illustrating the feasibility of rMBG particles as new DNA vectors, though a certain gap existed compared with the positive control groups.

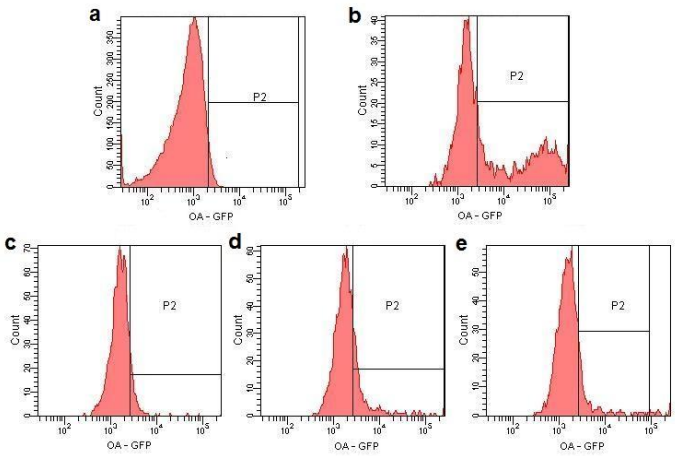

Fig.14. Flow cytometry of OA-GFP intensity in 293T cells transfected by rMBG-NH_2. (a)Control (b) Lipofectamin ™ 2000+pOA-GFP (c-e) pOA-GFP=5μg/mL, rMBG-NH_2/ pOA-GFP=20, 50 and 100 respectively.

4 Discussion

MBGs lead to a new family of biomaterials. MBGs possess higher specific surface area, accelerating the possible interactions with other materials/molecules and biological reactions.[7,36,51] The surface properties of nanoscale MBGs allow not only a faster release of ions but also a higher molecule adsorption.[4,52,53] The Si–OH groups on the surface of MBGs and the nanopores will help bind small-molecule drugs and proteins.[37] The characteristics of mesopores, including pore size, volume, and surface area, are very important in determining the capacity of the MBGs to incorporate and release candidate therapeutic molecules. In this study, we prepared special rMBG particles with mesoporous structures using CPB templates. The formation mechanism of rMBGs was illustrated in Fig.1. A possible formation mechanism[50]: in the micro-emulsion system, the fibrous template molecules are assembled by the surfactant micelles; the hydrolyzed TEOS are polymerized and formed negatively charged silicate molecules in the space among the fibrous template molecules; calcium cations are absorbed to the silicate via electrostatic interaction. Then, after condensation of the silicate, the Si-O networks are formed with the fibrous template molecules. Finally, rMBG particles are obtained by calcination.

MBG particles have higher specific surface area and surface energy compared with conventional powder BG materials. They attracted researchers due to their special characters and advantages.[21,54,55] In previous studies, the synthesized BG nanoparticles usually exhibited an agglomerated morphology. But, as we know, the dispersity of the particles plays a very important role in the drug delivery systems，which may have an significant influence on the drug-loading efficiency and the amount of cellular uptake. Therefore, it is important to obtain BG particles with great dispersibility. In this study, the rMBGs were synthesized by microemulsion technique with higher surface area and controlled morphology. rMBGs exhibited a regularly spherical shape without obvious agglomeration, which made it suitable for carries and easily entering into cells. Fig. 2 demonstrated that the particles were well dispersed without large agglomerates observed through SEM and TEM analysis (Fig. 2). The mesopore volume (PV), mesopore size and surface area (SA) were 1.3cm^3/g, 10.77 nm and 483.98 m^2/g respectively.

rMBG particles showed a stable mesoporous structure, large pore volume and pore diameter, and large special surface area, which indicated that rMBGs may be useful in a variety of medical applications, such as drug delivery, implants for bone and dental restoration or regeneration, and bioactive coatings of metallic implants in tissue engineering. Does rMBG have a shot at becoming a gene carrier? By now, the application of MBGs for DNA gene delivery has not yet been reported. In this study, we first explored the capacity of rMBGs on DNA transfection. We chose pOA-GFP as a gene carrier model. The OA protein temporal expressed in osteoblasts[56] is associated with the differentiation and maturation of osteoblasts by stimulating osteoblast differentiation markers, including alkaline phosphatase (ALP) activity, nodule formation, osteocalcin production, and matrix mineralization.[57-59] Blocking the function of OA with an antibody reduces the differentiation and functional activity of rat osteoblasts, without affecting cell proliferation and viability.[60] OA and BMP-2 have similar pattern of expression during osteoblast development in culture. A recent study indicated that OA acts as a downstream mediator of BMP-2 and affects osteoblast development and function.[61] So OA is an appropriate molecule chosen to be as a target gene delivered by rMBG vehicles.

Whether rMBGs are suitable for gene transfection depends on many conditions. Transfection process is complicated. To be a gene carrier, rMBG must possess many other properties, such as good biocompatibility, highly sustained DNA loading ability, protection DNA from degradation, successfully entering cells, escaping from lysosomal, and super releasing efficiency of genes in cells. Then the genes can be replicated, transcribed, and finally translated into proteins. Further studies were carried out on the capacity of rMBG particles on gene transfection.

According to our result, the rMBG particles had good biocompatibility, and could successfully enter into the cells in a dose- and time-dependent manner. Figure 6 exhibited that more than 90% cells expressed rMBG-FITC after 24 h incubation. Most of the particles were localized in cytoplasm. Even in the cells, the sea hedgehog-like structure of the particles was identified clearly (Fig.8).

rMBGs, as well as plasmid DNA, were negatively charged in physiological environment. They were mutually exclusive and rMBGs could not be directly used for adsorption of the plasmid. It was necessary to endow rMBGs with high DNA loading capabilities. The unique radial pore structure and large surface area with a large

number of Si–OH groups on the surface provided the rMBGs many potential surface modification sites. Various functional groups could easily be grafted on the rMBGs to change their electrical properties. In our study, amino modification of rMBGs was prepared with APTES in order to increase the gene loading efficiency. The zata potential and gel electrophoresis results showed that rMBG-NH_2 had a positive charge, ensure its capacity to load pOA-GFP plasmid DNA. Furthermore, rMBG-NH_2 could protect pOA-GFP from DNase I cleaving. These results indicated the positive interaction between rMBG-NH_2 and DNA.

rMBG had a high DNA loading ability and could protect DNA from degradation. This may be because that the large quantity of mesopores is considered highly beneficial for providing enough space to home DNA in large amounts. Next , gene transfected efficiency of rMBGs was measured by a microscope. OA-GFP fluorescence successfully detected in all rMBG transfected cells, and the rMBG-NH_2/pOA-GFP ratio=50 group achieved the best results, consistent with the data of flow cytometry. Therefore, we may draw a conclusion that the rMBG material we prepared were shown to be a promising novel non-viral vehicle in delivering target genes.

However, the gene transfection efficiency of rMBG still could not compete with the commoditized liposome transfection reagent. Furthermore, positive transfection proportion was not completely consistent with the percentage of the cells, in which rMBG particles were detected. The presence of the particles can be detected in more than 90% cells, while the corresponding gene expression rate was relatively low. This may be due to several reasons: 1) the plasmid containing OA and GFP fusion gene was relatively large, resulting in relatively low expression efficiency; 2) lysosomal escape capability of MBG is lower than that of liposome; 3) DNA adsorption rate of the particles could reach 100%, but the DNA might not be released from the particles rapidly after phagocytosis by cells. Because rMBG possessed rich mesopores, high surface area and pore volume, the nanopore structure in rMBG particles helped to bind with DNA. And another factor may be the amino-groups on the surface of rMBG-NH_2. They increased the DNA loading efficiency and prevented the rapid release of DNA in cells. The sustained release may avoid over expression of DNA and the possible side effects, while all of these need further experiments to confirm.

5 Conclusions

In this study, a novel type of rMBG particles were successfully synthesized by sol-gel process combining micro-emulsion method and gelation-induced phase separation technology with CPB templates. The particles were special, and possess many radical fibers and internal mesoporous structure. So the particles were density in the core and were loose around. rMBG particles showed a stable mesoporous structure, large pore volume and pore diameter, and large special surface area, which possessed highly DNA loading efficiency and sustained release properties. Based on the current results, rMBG were shown to be promising novel non-viral vehicles in delivering target genes such as bone-related genes for the bone repair and regeneration.

Acknowledgements

This work was supported by the National Natural Science Foundation of China (Grant No.51072055, 51172073, 51202069), Key Project of the National Natural Science Foundation of China (Grant No.50830101), the National Program on Key Basic Research Project of China (973 Program) (2011CB606204, 2012CB619100), the Doctoral Fund of Ministry of Education of China (20110172110002) and the Fundamental Research Funds for the Central University (No.2014ZM0009, 2012ZP0001,2013ZM0043).

Notes and references

[a] School of Materials Science and Engineering, South China University of Technology, Guangzhou 510641, China.
[b] National Engineering Research Center for Tissue Restoration and Reconstruction, South China University of Technology, Guangzhou 510006, China.
[c] Key Laboratory of Biomedical Materials and Engineering, Ministry of Education, Guangzhou 510006, China.
* Corresponding author. School of Materials Science and Engineering, South China University of Technology, Guangzhou 510641, China. E-mail address: chenxf@scut.edu.cn (X. Chen)

References:

1 J. R. Porter, T. T. Ruckh and K. C. *Popat, Biotechnol. Prog.*, 2009, **25**, 1539-1560.
2 A. R. Amini, C. T. Laurencin and S. P. Nukavarapu, Crit. *Rev. Biomed. Eng.*, 2012, **40**, 363-408.
3 M. Stevens, Mater. Today, 2008, **11**, 18-25.
4 J, Will, L. C. Gerhardt and A. R. Boccaccini, *Adv. Biochem. Eng. Biotechnol.*, 2012, **126**, 195-226.
5 L. L. Hench, R. J. Splinter, W. C. Allen and T. K. Greenlee, *J. Biomed. Mater. Res.*, 1971, **5**, 117-141.
6 D. L. Wheeler, M. J. Montfort, S and W. McLoughlin, *J. Biomed. Mater. Res.*, 2001, **55**, 603-612.
7 A. R. Boccaccini, M. Erol, W. J. Stark, D. Mohn, Z. Hong and J. F. Mano, *Compos. Sci. Technol*., 2010, **70**, 1764-1776.
8 L. L. Hench, *J. Mater. Sci., Mater. Med*., 2006, **17**, 967–978.
9 L. L. Hench, Bioceramics, *J. Am. Ceram. Soc.*, 1998, **81**, 1705-1728.
10 B. Lei, L. Wang, X. Chen and S. K. Chae, *J. Mater. Chem. B*, 2013,**1**, 5153-5162.
11 C. Xu, P. Su, X. Chen, Y. Meng, W. Yu , A. P. Xiang and Y. Wang, *Biomaterials*, 2011,**32**, 1051-1058.
12 I. Christodoulou, L .D. Buttery, P. Saravanapavan, G. Tai, L. L. Hench and J. M. Polak, *J. Biomed. Mater. Res B.* Appl Biomater, 2005, **74**, 529-537.
13 L. L. Hench, I. D. Xynos and J. M. Polak, J. Biomat. *Sci., Polym. Ed.*, 2004, **15**, 543–562.
14 A. Hoppe, N. S. Güldal and A. R. Boccaccini, *Biomaterials*, 2011, **32**, 2757–2774.
15 I. D. Xynos, A. J. Edgar, L. D. Buttery, L. L. Hench and J. M. Polak, *Biochem. Biophys. Res. Commun.*, 2000, **276**, 461-465.
16 I. D. Xynos, A. J. Edgar and L. D. Buttery, *J. Biomed. Mater. Res.*, 2001, **55**, 151-157.
17 G. Jell and M. M. Stevens, *J. Mater. Sci. Mater. Med.*, 2006, **17**, 997–1002.
18 A. Gorustovich, J. Roether and A. R. Boccaccini, *Tissue. Eng. Part B. Rev*., 2010, **16**, 199–207.
19 L. C. Gerhardt, K. L. Widdows, M. M. Erol, C. W. Burch, J. A. Sanz - Herrera, I. Ochoa, R. Stämpfli, I. S. Roqan, S. Gabe, T. Ansari and A.R. Boccaccini, *Biomaterials*, 2011, **32**, 4096–4108.
20 R. M. Day. *Tissue. Eng*., 2005, **11**, 768–777

21 M. N. Rahaman, D. E. Day, B. S. Bal, Q. Fu, S. B. Jung, L. F. Bonewald and A. P. Tomsia, *Acta. Biomater*., 2011, **7**, 2355–2373.
22 R. Li, A. E. Clark and L. L. Hench, *J. Appl. Biomater.*, 1991, **2**, 231–239.
23 X. Yan, C. Yu, X. Zhou, J. Tang and D. Zhao, *Angewandte. Chemie.*, 2004, **43**, 5980-5984.
24 Q. Jie, K. Lin, J. Zhong, Y. Shi, Q. Lin, J. Chang and R.Wang, *Sci. Technol.*, 2004, **30**, 49–61.
25 I. Izquierdo-Barba, A. J. Salinas and M. Vallet-Reg ί, *Int. J. Appl. Glass. Sci.*, 2013, **4**, 149-161.
26 Y. Zhu and S. Kaskel, Microporous. *Mesoporous. Mater*., 2009, **118**, 176–182.
27 C. Wu and J, *Interface. Focus.*, 2012, **2**, 292-306.
28 B. Lei, X. Chen, X. Han and Z. Li, *J. Mater. Chem.*, 2011, **21**, 12725-12734
29 Q. Hu, X. Chen, N. Zhao and Y. Li, *Mater. Lett.*, 2013, **106**, 452-455.
30 Q. Hu, X. Chen, N. Zhao, Y. Li and C. Mao, *J. Sol-Gel. Sci. Techn.*, 2014, **69**, 9-16.
31 G. Miao, X. Chen, H. Dong, L. Fang, C. Mao, Y. Li, Z. Li and Q. Hu, *Mater. Sci. Eng C., Mater. Biol. Appl*., 2013, **33**, 4236-4243.
32 B. Lei, X. Chen, X. Han and J. Zhou, *J. Mater. Chem.*, 2012, **22**, 16906-16913.
33 A. El-Fiqi, T. H. Kim, M. Kim, M. Eltohamy, J. E. Won, E. J. Lee and H. W. Kim, *Nanoscale*, 2012, **4**, 7475–7488.
34 J. K. Christie and A. Tilocca, *J. Mater. Chem.*, 2012, **22**, 12023-12031
35 H. M. Lin, H. Y. Lin and M. H. Chan, *J. Mater. Chem B.*, 2013, **1**, 6147-56.
36 C. T. Wu, W. Fan and J. Chang, *J. Mater. Chem B.*, 2013, **1**, 2710-2718.
37 C. Wu, J. Chang and W. Fan, *J. Mater. Chem.*, 2012, **22**, 16801-16809.
38 C. Wu, W. Fan, J. Chang and Y. Xiao, *J. Biomater. Appl.*, 2013, **28**, 367-374.
39 J. K. Leach, D. Kaigler, Z. Wang, P. H. Krebsbach and D. J. Mooney, *Biomaterials*, 2006, **27**, 3249–3255.
40 J. Zhang, H. J. Zhou, K. Yang, Y. Yuan and C. S. Liu, *Biomaterials*, 2013, **34**, 9381-9392.
41 C. Dai, H. Guo, J. Lu, J. Shi, J. Wei and C. Liu, *Biomaterials*, 2011, **32**, 8506–8517.
42 L. Xia, D. Zeng, X. Sun, Y. Xu, L. Xu, D. Ye, X. Zhang, X. Jiang and Z. Zhang, *Micropor. Mesopor. Mat.*, 2013, **173**, 155-165.
43 J. Wu, D. Yamanouchi, B. Liu and C. C. Chu, *J. Mater. Chem.*, 2012, **22**, 18983-18991.
44 W. Qu, S. Y. Qin, Y. Kuang, R. X. Zhuo and X. Z. Zhang, *J. Mater. Chem. B*, 2013, **1**, 2147-2154.
45 M. Morille, C. Passirani, A. Vonarbourg, A. Clavreul and J. P. Benoit, *Biomaterials*, 2008, **29**, 3477-3496.
46 S. B. Hartono, N. T. Phuoc, M. Yu, Z. Jia, M.l J. Monteiro, S. Qiao and C. Yu, *J. Mater. Chem. B*, 2014, **2**, 718-726.
47 K. W. Leong, H.Q. Mao, V. L. Truong-Le, K. Roy, S. M. Walsh and J.T. August, *J. Controlled. Release.*, 1998, **53**, 183–193.
48 F. P. Chang, L. Y. Kuang, C. A. Huang, W. N. Jane, Y. Hung, Y. C. Hsing and C. Y. Mou, *J. Mater. Chem. B*, 2013, **1**, 5279-5287.
49 F. F. Safadi, J. Xu, S. L. Smock, M. C. Rico, T. A. Owen and S. N. Popoff. *J. Cell. Biochem.*, 2001, **84**, 12-26.
50 D. S. Moon and J. K. Lee, *Langmuir*, 2012, **28**, 12341-12347
51 M. Erol-Taygun, K. Zheng and A. R. Boccaccini, *Int. J. Appl. Glass. Sci.*, 2013, **4**, 136-148.
52 X. Li, J. L. Shi, X. P. Dong, L. X. Zhang and H. Y. Zeng, *Biomed. Mater. Res.*, 2007, **84A**, 84–91.
53 H. M. Lin, Y. H. Lin and F. Y. Hsu, *J. Mater. Sci., Mater. Med.*, 2012, **23**, 2619-2630.
54 R. A. Perez, T. H. Kim, M. Kim, J. H. Jang, M. P. Ginebra and H. W. Kim, J. Biomed. *Mater. Res. Part A*., 2013, **101A**, 923–931.
55 M. Ahmad, J. R. Jones and L. L. Hench, *Biomed. Mater*., 2007, **2**, 6-10.
56 S. M. Abdelmagid, M. F. Barbe, M. Hadjiargyrou, T. A. Owen, R. Razmpour, S. Rehman, S. N. Popoff and F. F. Safadi, *J. Cell. Biochem.*, 2010, **111**, 295–309.
57 A. A. Selim, J. L. Castaneda, T. A. Owen, S. N. Popoff, F. F. Safadi, *Med. Sci. Monit*., 2007, **13**, BR259-270.
58 G. R. Sondag, S. Salihoglu, S. L. Lababidi, D. C. Crowder, F. M. Moussa, S. M. Abdelmagid and F. F. Safadi, *J. Cell. Physiol*., 2014, **229**, 955–966.
59 F. M. Moussa, I. A. Hisijara, G. R. Sondag, E. Scott, N. Frara, S. M. Abdelmagid and F. F. Safadi, *J. Cell. Biochem.*, 2014, Accepted Article (DOI: 10.1002/jcb.24760). Available from URL: http://onlinelibrary.wiley.com/doi/10.1002/jcb.24760/pdf
60 A. A. Selim, S. M. Abdelmagid, R. A. Kanaan, S. L. Smock, T. A. Owen, S. N. Popoff and F. F. Safadi, *Crit. Rev. Eukaryot. Gene. Expr*., 2003, **13**, 265-275.
61 S. M. Abdelmagid, M. F. I. Barbe, Arango-Hisijara, T. A. Owen, S. N. Popoff, F. F. Safadi, *J. Cell. Physiol.*, 2007, **210**, 26-37.

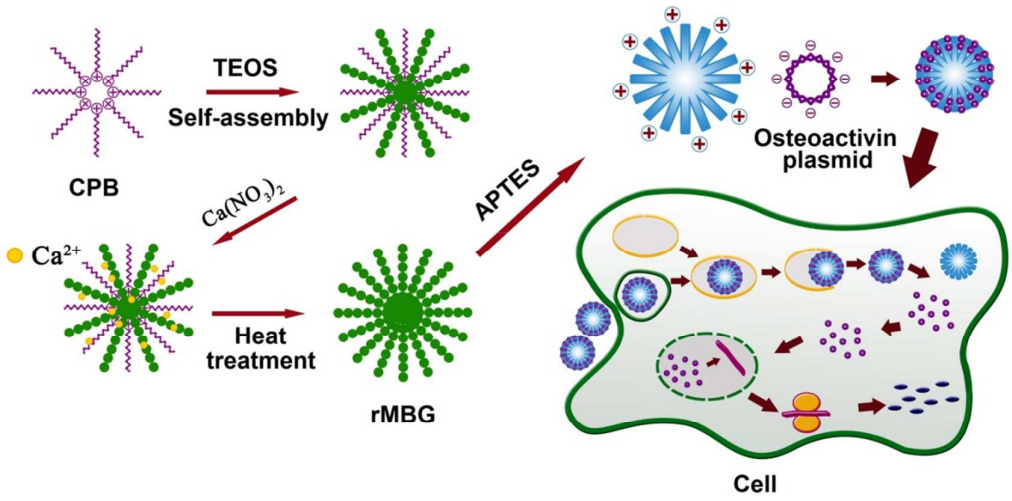

HIGHLIGHT

Synthesis of radical mesoporous bioactive glass particles to deliver osteoactivin gene.